Computational Materials Science 142 (2018) 47–58

Contents lists available at ScienceDirect

Computational Materials Science

journal homepage: www.elsevier.com/locate/commatsci

An interatomic potential for the Li-Co-O ternary system

Eunkoo Lee [a], Kwang-Ryeol Lee [b], Byeong-Joo Lee [a,*]

[a] Department of Materials Science and Engineering, Pohang University of Science and Technology (POSTECH), Pohang 37673, Republic of Korea
[b] Computational Science Center, Korea Institute of Science and Technology, Seoul 02792, Republic of Korea

ARTICLE INFO

Article history:
Received 23 July 2017
Received in revised form 28 September 2017
Accepted 3 October 2017
Available online 13 October 2017

Keywords:
Interatomic potential
Molecular dynamics
Modified embedded atom method
Charge equilibration
Lithium cobalt oxide
$LiCoO_2$
Diffusion coefficient
Lithium diffusion
Lithium ion battery

ABSTRACT

Although large-scale atomistic simulations provide useful insights into various material phenomena, such studies on $LiCoO_2$, which is the most widely used cathode material for lithium ion batteries (LIBs), have rarely been undertaken due to difficulties in developing adequate interatomic potentials. In this study, an interatomic potential (2NNMEAM + Qeq) for the Li-Co-O ternary system is developed to carry out molecular dynamics (MD) simulation studies on lithium cobalt oxides. Potential parameters are optimized so that the potential can successfully reproduce fundamental materials properties (structural, elastic, thermodynamic and migration properties) of various compounds of sub-binary and lithium cobalt ternary oxide systems. Through MD simulations, we investigate lithium diffusion properties (activation energy for lithium migration and diffusion coefficient) in layered $Li_{1-x}CoO_2$ ($0 \leq x \leq 0.5$) of various lithium vacancy concentrations. We find that the lithium vacancy concentration has a significant influence on the activation energy for lithium diffusion and the lithium diffusion coefficient in the $Li_{1-x}CoO_2$ cathode. The developed potential can be further utilized for atomistic simulation studies on other materials phenomena (phase transitions, defect formation, lithiation/delithiation, etc.) in LIB cathode materials.

1. Introduction

$LiCoO_2$ is the most widely used cathode material for lithium ion batteries (LIBs) because of its advantages such as fast Li-ion migration, high voltage and high capacity. However, because of the high material cost and toxicity of the Co element, searching for replacement cathode materials that have a lower cobalt content has attracted recent research interest [1,2]. Although various cathode materials have been proposed including solid solutions of Li-(Co, Mn, Ni, Al, etc.)-O, there have been difficulties in finding a satisfactory replacement cathode material that has sufficiently good performance in the areas of structural stability, capacity, cyclic properties, and so on. One of the most important properties of LIB cathode materials is the lithium diffusion, the main determinant for the charge/discharge rate. However, there is a limit to accurately measuring the Li diffusion coefficient through experiments because of the nature of the very light element and no suitable radioisotope for Li [3]. In addition, investigating properties such as defect formation, lithiation/delithiation and phase transitions in various LIB cathode materials through experiments is difficult because they have atomic-scale origins. Such experiments are also inefficient because the number of possible compounds and doping elements for the cathode materials is almost limitless.

On the other hand, computational approaches can be efficiently utilized for investigations of a wide range of materials phenomena. Among the approaches, the density functional theory (DFT) calculation is a high-level calculation that provides the most accurate information on (sub-)atomic-scale behaviors. However, the DFT calculation is not suitable for investigating dynamic behavior such as diffusion properties because of the limited number of atoms that can be handled. In this case, it is more appropriate to conduct large-scale atomistic simulations using a (semi-)empirical interatomic potential. However, there have been relatively few atomistic simulation studies on the LIB cathode materials. This is because of the difficulty in developing suitable interatomic potential models (and parameterization) for the LIB cathode materials, not because of a lesser importance of atomistic simulations.

The potential model applicable to LIB cathode materials systems should be able to cover various bonding natures (metallic, covalent and ionic bonds) in multi-component lithium transition metal oxide systems. In addition, it should be able to describe how the charge state of individual ions can change in redox reactions during the charge/discharge process. However, most previous studies [4–12] used a simple pair-wise type potential coupled with a fixed charge model. The pair-wise potential cannot cover com-

* Corresponding author.
E-mail address: calphad@postech.ac.kr (B.-J. Lee).

https://doi.org/10.1016/j.commatsci.2017.10.010
0927-0256/

plex bonding natures, and the fixed charge model simply considers the charge states of ions to be fixed during simulations. In recent years, to extend the materials coverage of the potential model, many-body type potentials coupled with a variable charge model have been developed: reactive force-field (ReaxFF) [13,14], charge optimized many-body (COMB) [15,16], charge transfer modified embedded-atom method (CT-MEAM) [17,18] and second nearest-neighbor MEAM coupled with charge equilibration (2NNMEAM + Qeq [19]). However, there are only a few applications of that kind of potential model to LIB cathode material systems [17,18,20], and there is no application to the Li-Co-O system, which is one of the most essential cathode material systems.

Our group have developed the 2NNMEAM + Qeq potential model to extend the coverage of the existing 2NNMEAM potential to multi-component metal oxide systems [19]. Based on this potential formalism, we have developed an Li-Mn-O ternary potential recently [20] and are constructing a potential database for LIB cathode material systems. The main objective of this study is to develop the Li-Co-O ternary potential. This is the first achievement for the Li-Co-O system, based on a many-body potential with variable charge scheme. We report the result of MD simulation on lithium diffusion properties in a layered $Li_{1-x}CoO_2$ cathode using the developed potential. Section 2 gives a brief description of the 2NNMEAM + Qeq potential model. Section 3 reports on the evaluation of the developed potentials for the sub-binary systems (Li-Co and Co-O) and ternary Li-Co-O system. Section 4 discusses the results of the MD simulation on lithium diffusion in layered $Li_{1-x}CoO_2$.

2. The 2NNMEAM + QEQ potential

The 2NNMEAM [21,22], one of the latest versions of MEAM [23–25], has been applied to a wide range of materials including metals, covalent elements and their alloys. In particular, it has been successfully applied to essential metallic elements associated with LIB cathode materials, such as Li [26], Co [27], Mn [28], Ni [29], Al [29] and some of their alloys. Recently, our group further extended the 2NNMEAM to cover multicomponent oxide compounds by combining it with a charge equilibration (Qeq [30]) concept (2NNMEAM + Qeq) [19]. Special attention was given to the removal of known problems found in the original Qeq method, during the implementation of the Qeq to the 2NNMEAM.

The total energy of a system in the 2NNMEAM + Qeq potential model [19] is composed of non-electrostatic (2NNMEAM) and electrostatic (Qeq) energy terms, as in the following expression.

$$E^{Total} = E^{MEAM}(\mathbf{r}) + E^{ES}(\mathbf{r}, \mathbf{q}) \tag{1}$$

The MEAM energy is calculated as

$$E^{MEAM} = \sum_i \left[F_i(\bar{\rho}_i) + \frac{1}{2}\sum_{j\neq i} S_{ij}\phi_{ij}(R_{ij}) \right] \tag{2}$$

where F_i is the embedding function, ρ_i is the background electron density at site i. S_{ij} and $\phi_{ij}(R_{ij})$ are the screening factor and the pair interaction between atoms i and j separated by a distance R_{ij}, respectively. Full details of the MEAM energy term are not included in this paper, and can be found in the literature [21,22] or in the electronic supplementary information (ESI) of this paper.

The electrostatic energy is expressed as the sum of atomic energy E_i^{atom} (or penalty energy) and the Coulomb pair interaction V_{ij}^{Coul}:

$$E^{ES} = \sum_i E_i^{atom}(q_i) + \sum_{i,j(i\neq j)} \frac{1}{2} V_{ij}^{Coul}(q_i, q_j, R_{ij}) \tag{3}$$

where q_i is the charge state of atom i. The charge state of each atom is not fixed but variable depending on the local environment. Our model use a quadratic spline function of q_i for E_i^{atom} [19], and Coulomb integral between two density functions of the 1s-Slater orbital [31] for V_{ij}^{Coul}. In addition, our potential formalism uses the concept of the split-charge [32], $\bar{q}_{ji}$, which represents the charge flow from the covalently bonded neighbor atom j to the atom i. Full details on the mathematics and algorithms for computing the equilibrium charge using our potential model can be found in Ref. [19] or in the ESI of this paper.

The potential formalism requires the following parameters: fifteen 2NNMEAM parameters (E_c, R_e, α, A, $t^{(1)-(3)}$, $\beta^{(0)-(3)}$, C_{min}, C_{max}, d_{rep} and d_{att}) and seven Qeq parameters (χ^0, J^0, $\Delta E^{(2)-(4)}$, ζ and Z) for each element. Fourteen and six parameters are also required for each pair and triplet, respectively (only the 2NNMEAM part): ΔE_c, R_e, α, d_{rep}, d_{att}, C_{min} (i-j-i), C_{min} (j-i-j), C_{min} (i-i-j), C_{min} (i-j-j), C_{max} (i-j-i), C_{max} (j-i-j), C_{max} (i-i-j), C_{max} (i-j-j) and $\rho_0(i)/\rho_0(j)$) for i-j pair, and C_{min} (i-k-j), C_{min} (i-j-k), C_{min} (j-i-k), C_{max} (i-k-j), C_{max} (i-j-k) and C_{max} (j-i-k) for i-k-j triplet. The Qeq part of our model operates only when a charge is assigned to the atoms in the system. This means that unary or metallic alloy systems are described only by the pristine 2NNMEAM formalism. Thus, we use the previously reported 2NNMEAM parameters of Li [26] and Co [27] without any modification. The 2NNMEAM and Qeq parameters for pure O are taken from a previous study on Ti-O and Si-O systems [19]. The Qeq parameters for pure Li and binary 2NNMEAM parameters for the Li-O pair had been determined during the development of the Li-Mn-O ternary potential in another previous study [20], and we use those parameters in this study. Therefore, a total of forty-one parameters (seven Qeq parameters for pure Co, fourteen binary 2NNMEAM parameters for each Li-Co and Co-O pair, and six ternary 2NNMEAM parameters for Li-Co-O triplet) are optimized in this study. The optimization of the parameters is performed using a genetic algorithm (GA). The finally selected potential parameters are listed in Table 1. The cutoff distances for 2NNMEAM and Coulomb interaction are taken as 4.8 Å and 12.0 Å, respectively.

3. Evaluation of the potential development

The reliability of the atomistic simulation results depends on the accuracy of the interatomic potential used in the simulation. In this section, we evaluate whether the developed potential correctly reproduces various fundamental material properties of the relevant material systems (Li-Co, Co-O and Li-Co-O). The reproduced properties are divided into two groups. One includes target properties fitted in a parameter optimization process: lattice parameters, elastic constants, enthalpy of formation and lithium migration energy barrier. The other involves properties calculated to check the transferability of the potential, which are not fitted: redox potential and defect formation energies. In addition, we check whether the developed potential remains reliable in finite temperature simulations as well as in zero K calculations. We use our own in-house code for all calculations, and the source code is included in the ESI of this paper. During all calculations, the charge on individual atoms is automatically determined according to the atomic environment by the Qeq scheme. No charge is assigned to Li and Co atoms in Li-Co alloys. Co atoms have the charge within the range of +1.04 and +1.09, and O atoms between −1.04 and −0.55 in $Co_{1-x}O_x$ ($1/2 \le x \le 2/3$). In Li_xCoO_2 ($0 \le x \le 1$) compounds, the charge of Li, Co and O atoms are between 0 and +0.42, between +1.09 and +1.08, and between −0.55 and −0.74, respectively.

Table 1
2NNMEAM + Qeq parameters for pure Li, Co and O, Li-Co, Li-O and Co-O pair, and Li-Co-O triplet. 2NNMEAM parameters (E_c, R_e, α, d_{rep}, d_{att}, A, $t^{(1)-(3)}$, $\beta^{(0)-(3)}$, C_{min}, C_{max}) for pure Co [27], and all parameters for Li [20], O [19], Li-O [20] are as published in literature. Qeq parameters (χ^0, J^0, $\Delta E^{(2)-(4)}$, ζ, Z) for Co, and 2NNMEAM parameters for Li-Co, Co-O and Li-Co-O were optimized in this study.

Element	Li	Co	O	*i-j* pair	Li-Co	Li-O	Co-O
Reference	bcc	hcp	dimer	Reference	b1	b1	b1
E_c (eV/atom)	1.65	4.41	2.56	E_c (eV/atom)	2.12	1.68	1.79
R_e (Å)	3.02	2.50	1.21	R_e (Å)	2.31	1.95	2.08
α	3.10	5.24	6.88	α	3.98	7.32	6.10
d_{rep}	0.05	0.00	0.00	d_{rep}	0.00	0.07	0.02
d_{att}	0.05	0.00	0.00	d_{att}	0.00	0.07	0.00
A	0.95	0.90	1.44	C_{min} (*i-j-i*)	1.80	1.00	4.00
$t^{(1)}$	2.30	3.00	0.10	C_{min} (*j-i-j*)	0.16	0.30	0.10
$t^{(2)}$	5.00	5.00	0.11	C_{min} (*i-i-j*)	0.30	0.70	0.50
$t^{(3)}$	0.50	−1.00	0.00	C_{min} (*i-j-j*)	0.30	0.60	0.50
$\beta^{(0)}$	1.65	3.50	5.47	C_{max} (*i-j-i*)	3.60	1.55	5.00
$\beta^{(1)}$	1.00	0.00	5.30	C_{max} (*j-i-j*)	2.80	1.55	1.80
$\beta^{(2)}$	4.00	0.00	5.18	C_{max} (*i-i-j*)	2.80	1.35	4.00
$\beta^{(3)}$	1.00	4.00	5.57	C_{max} (*i-j-j*)	2.80	2.15	4.00
C_{min}	0.16	0.49	2.00	$\rho_0(j)/\rho_0(i)$	2.0	24.0	12.0
C_{max}	2.80	2.00	2.80	*i-j-k* triplet	Li-Co-O		
χ^0 (eV/*e*)	−9.50	1.87	10.11	C_{min} (*i-k-j*)	1.20		
J^0 (eV/e^2)	50.0	9.42	20.5	C_{min} (*i-j-k*)	4.00		
$\Delta E^{(2)}$ (eV)	50	35	5.63	C_{min} (*j-i-k*)	2.50		
$\Delta E^{(3)}$ (eV)	–	50	50	C_{max} (*i-k-j*)	4.10		
$\Delta E^{(4)}$ (eV)	–	–	–	C_{max} (*i-j-k*)	6.00		
ζ (Å^{-1})	10.0	4.0	2.39	C_{max} (*j-i-k*)	5.00		
Z (*e*)	0.00	0.00	0.00				

3.1. Evaluation of the Li-Co potential

In the Li-Co binary system, there is no stable compound to be considered for parameter optimization. Therefore, we determine the parameters for the Li-Co pair by fitting the equation of state (EOS) for a hypothetic phase of the B1 structure and the enthalpy of formation (ΔH_f) of hcp-Li_xCo_{1-x} solid solutions to DFT calculations. We perform the DFT calculations using the Vienna ab initio simulation package (VASP) [33] within the project-augmented wave (PAW) [34] method. The generalized gradient approximation Perdew-Burke-Ernzerhof (GGA-PBE) exchange and correlation functional are applied to all calculations [35]. The plane wave cut-off energy is 520 eV. Self-consistent calculations are done by the tetrahedron method with Blöchl correlations [36]. An effective on-site Hubbard U_{eff} of 3.32 eV for Co ions is included in all calculations [37].

In the lithium cobalt binary alloy, the charge state of metal atoms is neutral because the charge flow (or split-charge) between metal elements is not defined. Thus, the metallic alloy system is handled by the 2NNMEAM part only. Since the 2NNMEAM potential formalism reproduces the EOS for the given reference structure correctly by definition, the calculated EOS of B1 agrees well with the DFT calculation as shown in Fig. 1(a). In the case of the hcp-solid solution of Li_xCo_{1-x}, Niessen et al. [38] report that there is some solid solubility of Li in Co, and that the ΔH_f would have positive values. Although our calculation overestimates the DFT calculation in the entire composition range, it is coincident with the fact that ΔH_f is positive as shown in Fig. 1(b).

3.2. Evaluation of the Co-O potential

There are three cobalt oxides, CoO, Co_3O_4 and Co_2O_3 [39]. At ambient temperatures, CoO has an NaCl-type B1 crystal structure [40,41]. A zinc blende type B3 and a wurtzite type B4 structure of CoO have also been discovered from experiments [40,41]. Co_3O_4 is known to crystallize in the normal spinel structure [39,42,43]. It is known that CoO and Co_3O_4 have a small number of deviations from stoichiometry with cation defects. In this study, however, CoO and Co_3O_4 are treated as stoichiometric compounds. Co_2O_3 (corundum structure) appears to be stable only at low temperatures below 500–700 K or under high oxygen partial pressure [39,44]. In addition to the experimentally investigated phases, we

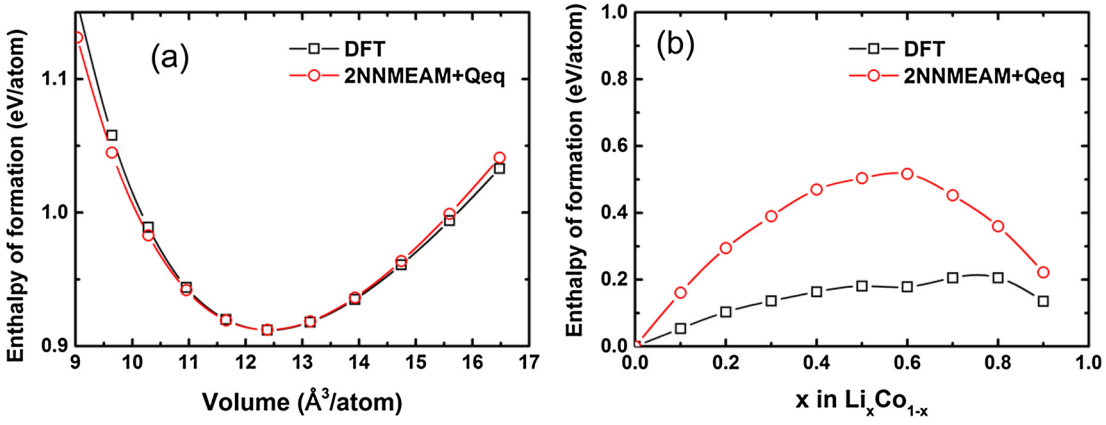

Fig. 1. (a) Equation of state of B2-LiCo as a function of volume and (b) enthalpy of formation of hcp-Li_xCo_{1-x} solid solution as a function of lithium concentration.

Table 2
Lattice parameters of cobalt oxide phases.

Phase		2NNMEAM + Qeq	% error	Expt.	DFT[f]
CoO B1	*a* (Å)	3.8691	−9.04	4.267[a] 4.24[b]	4.279
CoO B3	*a* (Å)	4.1679	−8.60	4.57[a] 4.55[b]	4.593
CoO B4	*a* (Å)	2.9786	−7.21	3.21[a] 3.21[b]	3.266
	c (Å)	4.8627	−7.20	5.24[a] 5.24[b]	5.276
Co_3O_4	*a* (Å)	7.9149	−2.08	8.086[c] 8.08[d]	8.152
Co_2O_3	*a* (Å)	4.8507	−0.64	4.882[e]	5.037 [g]
	c (Å)	13.0118	−2.75	13.38[e]	13.413 [g]
Co_5O_8	*b* (Å)	8.1189	+0.47*		8.081
Layered Li_0CoO_2	*a* (Å)	2.9704	+4.59*		2.84
	c (Å)	14.8751	+4.30*		14.262
Spinel Li_0CoO_2	*a* (Å)	8.4060	+5.47*		7.97
CoO_2 (*I*4/*m*)	*a* (Å)	9.7749	+2.93*		9.497
	c (Å)	2.9771	+3.55*		2.875
CoO_2 (*Pmnb*)	*a* (Å)	2.9497	+2.81*		2.869
	b (Å)	8.8650	+6.69*		8.309
	c (Å)	10.1734	+2.49*		9.926
rRMSE (%)			5.43		

[a] Ref. [40].
[b] Ref. [41].
[c] Ref. [42].
[d] Ref. [43].
[e] Ref. [44].
[f] Ref. [37].
[g] Ref. [49].
* Relative error with respect to the DFT calculation.

Table 3
Bulk modulus (GPa) of cobalt oxide phases.

Phase	2NNMEAM + Qeq	DFT[a]
CoO B1	324	236
CoO B3	175	129
CoO B4	124	130
Co_3O_4	147	160
Co_2O_3	161	
Co_5O_8	88	140
Layered Li_0CoO_2	33	23
Spinel Li_0CoO_2	48	120
CoO_2 (*I*4/*m*)	90	69
CoO_2 (*Pmnb*)	92	134

[a] Ref. [37].

also consider five hypothetic phases that are predicted to be (meta-)stable by a DFT calculation [37]: Co_5O_8 (the same structure as cubic Mn_5O_8 [45], space group: $F\bar{4}3m$), layered Li_0CoO_2 (a fully delithiated structure of layered $LiCoO_2$ [46,47], space group: $R\bar{3}m$), spinel Li_0CoO_2 (a fully delithiated structure of spinel $LiCoO_2$ [48]), and two more CoO_2 phases of which the space group is *I*4/*m* and *Pmnb*. By including these hypothetical phases in the fitting procedure of the Co-O binary system, our final ternary potential should have a better performance in the ternary Li-Co-O system.

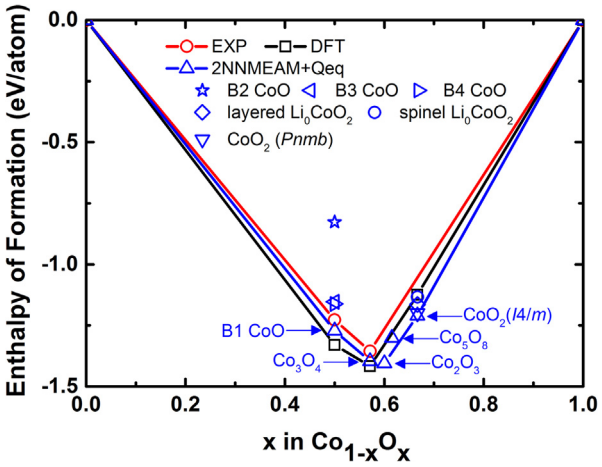

Fig. 2. Enthalpy of formation of cobalt oxide phases in comparison with experimental data [39] and a DFT calculation [37].

To evaluate whether the developed potential can reproduce the structural properties of cobalt oxide compounds, we compare the calculated lattice parameters of all the phases considered in the fitting procedure with experimental data [40–44] and DFT calcula-

Table 4
Elastic constants (GPa) of CoO phases.

	B1		B3		B4	
	2NNMEAM + Qeq	Exp.[a]	2NNMEAM + Qeq	DFT[b]	2NNMEAM + Qeq	DFT[b]
B	324	180.9	175	129	124	130
C_{11}	353	255.6	158	145	132	183
C_{12}	296	143.6	167	122	79	116
C_{44}	118	80.3	37	59	30	29
C_{13}					80	98
C_{33}					320	178
C_{66}					27	33

[a] Ref. [50].
[b] Ref. [37].

Table 5
Lattice parameters of lithium cobalt oxide phases.

Phase		2NNMEAM + Qeq	% error	Expt.	DFT
Layered $LiCoO_2$	a (Å)	2.7915	−0.90	2.8155[a] 2.8149[b]	2.8260[f] 2.8380[g]
	c (Å)	13.5927	−3.30	14.0550[a] 14.0525[b]	14.2070[f] 14.1730[g]
Spinel $LiCoO_2$	a (Å)	7.8365	−2.29	7.994[c]	
Layered $Li_{0.5}CoO_2$	a (Å)	5.0291	+3.32	4.865[d] 4.865[e]	4.897[g]
	b (Å)	2.7948	−0.46	2.806[d] 2.809[e]	2.947[g]
	c (Å)	4.6259	−8.75	5.093[d] 5.063[e]	5.098[g]
	β (°)	106.8090	−1.68	109.33[d] 108.68[e]	109.33[g]
Spinel $Li_{0.5}CoO_2$	a (Å)	8.0261	+0.43	7.992[c]	8.0310[f]
rRMSE (%)			3.03		

[a] Ref. [46].
[b] Ref. [47].
[c] Ref. [48].
[d] Ref. [51].
[e] Ref. [52].
[f] Ref. [53].
[g] Ref. [54].

Table 6
Bulk modulus (B) and enthalpy of formation (ΔH_f) of lithium cobalt oxide phases.

Phase	B (GPa)		ΔH_f (eV/atom)	
	2NNMEAM + Qeq	Ref.	2NNMEAM + Qeq	Ref.
Layered $LiCoO_2$	163	149[a1] 142.9[a2] 117[b]	−1.7140	−1.782[b] −1.762[c] −1.78[d]
Spinel $LiCoO_2$	165		−1.7018	
Layered $Li_{0.5}CoO_2$	135	89[b]	−1.4808	−1.499[b] −1.4390[c]
Spinel $Li_{0.5}CoO_2$	158		−1.5065	−1.457[b] −1.516[d]

[a] Ref. [46]: [1]Exp., [2]DFT.
[b] Ref. [37], DFT.
[c] Ref. [55], Exp.
[d] Ref. [53], DFT.

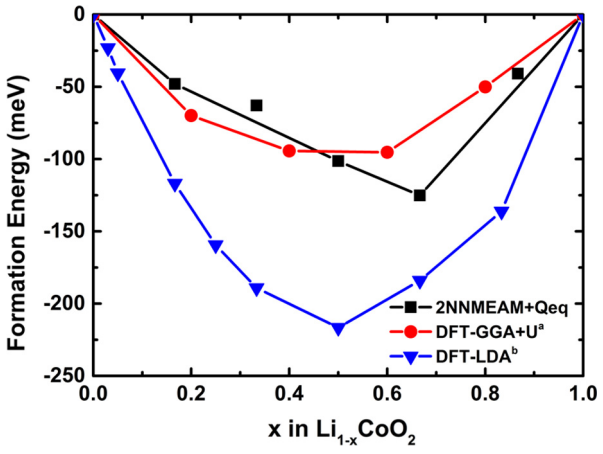

Fig. 3. Formation energy of delithiated $Li_{1-x}CoO_2$ (layered structure) in comparison with DFT calculations: [a]Ref. [56], [b]Ref. [57].

tions [37,49], as shown in Table 2. Our calculation for CoO phases underestimates the lattice parameters compared to the experimental data [40,41] by about 8% while those for Co_3O_4 and Co_2O_3 are in good agreement (around 2% error) with the experimental data [42–44]. The relative error of our calculation for the hypothetical phases is around 5% compared to the DFT calculations [37,49]. In overall, the calculated lattice parameter of cobalt oxide phases is within a reasonable error range (relative root mean squared error, rRMSE is 5.43%).

Table 3 shows the calculated bulk modulus of cobalt oxide phases in comparison with a DFT calculation [37]. The result is in an acceptable agreement with the DFT calculation. Table 4 shows the calculated elastic constants of CoO B1, B3 and B4 phases in comparison with experimental data [50] for B1 and a DFT calculation [37] for B3 and B4. Our potential reproduces the elastic constants of CoO B1, B3 and B4 well. To verify that our potential correctly reproduces energetics of lithium oxide phases, we compare the calculated enthalpy of formation, ΔH_f, with experimental data [39] and a DFT calculation [37] in Fig. 2. The calculated ΔH_f of CoO B1 and Co_3O_4 is between the experimental data and the DFT calculation. Our potential predicts that the B1 phase is energetically more stable than the B3 and B4 phases and also the hypothetical B2 phase. There is no available experimental data for ΔH_f of Co_2O_3, Co_5O_8 and CoO_2 phases. The ΔH_f of those phases are predicted within the overall tendency of the ΔH_f curve.

Although the calculated materials properties for the Co oxides are generally comparable to literature data, it needs to be mentioned here that our potential tend to underestimate the lattice constants for low valence Co oxides while shows the opposite for high valence Co oxides. This tendency had also been observed in our previous work for Mn oxides [20]. At this moment, it is hard to say the reason for the systematic error in lattice constants and even to say whether such an error characteristic is an inherent one in the 2NNMEAM + Qeq formalism or not. A continuous attention would need to be paid to this error characteristic in future works.

3.3. Evaluation of the Li-Co-O potential

The Li-Co-O ternary system contains the following phases: layered $LiCoO_2$ (hexagonal, space group: $R\bar{3}m$ [46,47]) and $Li_{0.5}CoO_2$ (monoclinic, space group: $P2/m$ [51,52]), and spinel $LiCoO_2$ (space group: $Fd\bar{3}m$) and $Li_{0.5}CoO_2$ (space group: $Fd\bar{3}m$) [48]. For the same purpose as in the Co-O binary system, we compare the calculated

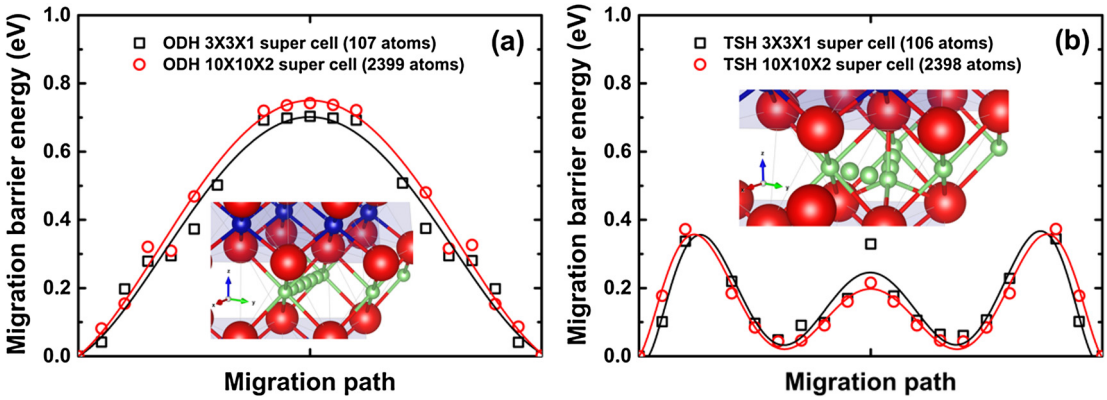

Fig. 4. Li migration energy barrier in layered $LiCoO_2$ according to two different migration pathways: (a) oxygen dumbbell hop (ODH) for hopping to an isolated vacancy site and (b) tetrahedral site hop (TSH) for hopping with a divacancy.

Table 7
Redox potentials (V) in lithium cobalt oxide phases.

Phase	2NNMEAM + Qeq	Expt.	DFT
Layered [$LiCoO_2$/$Li_{0.5}CoO_2$]	3.347	3.9[a], 3.85–4.0[b], 4.2[c]	3.75[d], 3.38[e1], 3.85[e 2], 4.51[e 3]
Spinel [$LiCoO_2$/$Li_{0.5}CoO_2$]	3.069	3.61[a], 3.3–3.9[b]	3.26[d]

[a] Ref. [68].
[b] Ref. [69].
[c] Ref. [70].
[d] Ref. [66], LDA.
[e] Ref. [67]: [1]GGA, [2]GGA + U, [3]HSE06.

fundamental materials properties (lattice parameters, elastic constants and enthalpy of formation) of Li-Co-O compounds with experimental data and/or DFT calculations. For practical applications, we check the reproducibility of the present potential for the lithium migration energy barrier and the redox potential. We also check the reliability of the potential at finite temperatures.

Table 5 shows calculated lattice parameters of lithium cobalt oxide phases in comparison with experimental data [46–48,51,52] and DFT calculations [53,54]. The present potential generally reproduces the lattice parameters well, and the relative root mean-squared error (rRMSE) is 3.03%. Table 6 summarizes the calculated bulk modulus, and the enthalpy of formation (ΔH_f) of lithium cobalt oxide phases is listed with the experimental data [46,55] and/or DFT calculations [37,46,53]. The present potential generally overestimates the bulk modulus of layered $LiCoO_2$ and $Li_{0.5}CoO_2$ compared to the DFT calculations. The calculated enthalpy of formation agrees well with the experimental data and DFT calculations. To validate that the present potential can describe the full-delithiation for $LiCoO_2$ cathode material, we calculate the formation energy of delithiated $Li_{1-x}CoO_2$ (layered) where $0 < x < 1$ and compare it with DFT calculations [56,57], as shown in Fig. 3. We consider all combinations for the removal of Li atoms in the $2 \times 2 \times 1$ supercell for delithiated $Li_{1-x}CoO_2$ and calculate the minimum energy at each lithium composition. The calculated formation energy of delithiated $Li_{1-x}CoO_2$ is comparable with a GGA + U calculation [56].

One of the main objectives of developing the potential is to utilize it for large-scale diffusion simulations at finite temperatures. As a way to see whether the potential can be utilize for the diffusion simulation, we calculate in advance the lithium migration energy barrier in layered $LiCoO_2$ at 0 K. Van der Ven et al. [58,59] proposed through a DFT calculation that there are two mechanisms of lithium migration path depending on the lithium-vacancy arrangement around the hopping ion in the layered $LiCoO_2$ unit cell (space group: $R\bar{3}m$). When a lithium atom hops into an isolated vacancy site, the migration occurs along a linear path passing through the oxygen dumbbell (oxygen dumbbell hop, ODH). If the lithium atom hops into a vacancy that is part of a divacancy,

Table 8
Defect formation energies of layered $LiCoO_2$.

Defect type	2NNMEAM + Qeq	DFT
Li Frenkel (*isolated*/*neighboring*, eV)	2.561/2.272	3.43[a] 3.19–3.72[b] 3.74[c] 9.87[*,i]
Co Frenkel (*isolated*/*neighboring*, eV)	4.301/2.266	1.836[d] 21.74[*,i]
O Frenkel (*isolated*/*neighboring*, eV)	6.635/4.777	9.01[*,i]
$Co_{Li}Li_{Co}$ (*isolated*/*neighboring*, eV)	1.616/1.626	2.34[c] 1.602[d] 2.79[*,i]
(0 0 0 1) surface (J/m^2)	0.770	0.6[e] 0.4–1.0[g] 0.774[h] 1.38[*,i]
(0 1 $\bar{1}$ 0) surface (J/m^2)	1.443	2.943[g] 3.13[*,i]
(1 1 $\bar{2}$ 0) surface (J/m^2)	0.979	2.387[f] 2.241[g] 2.95[*,i]

[a] Ref. [71].
[b] Ref. [72].
[c] Ref. [73].
[d] Ref. [74].
[e] Ref. [75].
[f] Ref. [76].
[g] Ref. [53].
[h] Ref. [77].
[i] Ref. [4].
[*] Calculation using empirical potential model (Born + Shell model).

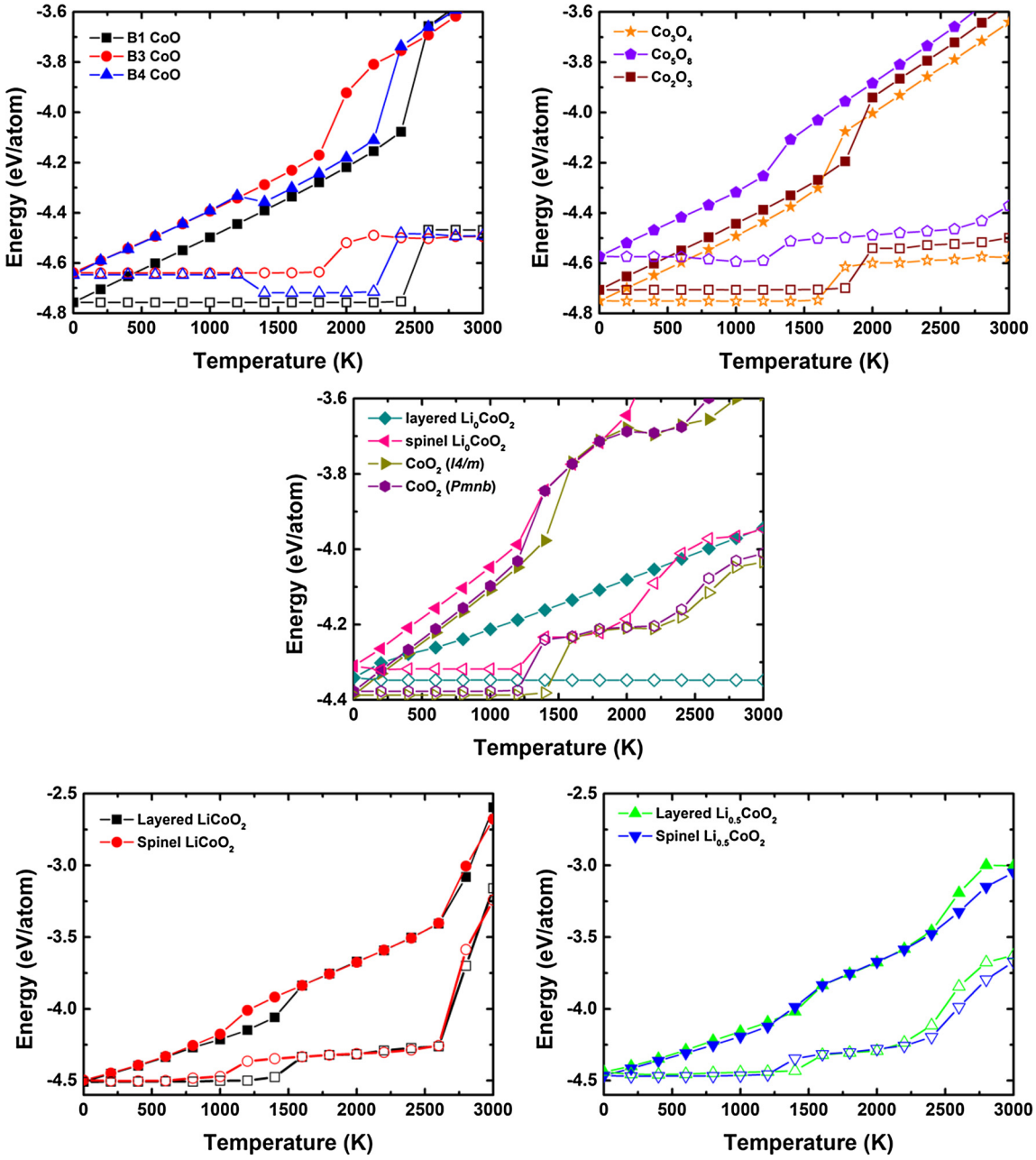

Fig. 5. Energy of cobalt oxide phases and lithium cobalt oxide phases as a function of temperature (solid symbol: during heating and open symbol: after rapid cooling to 0 K).

the migration occurs through the tetrahedral site, which is centered between the two vacancies and the initial site (tetrahedral site hop, TSH). We calculate the relative energy as a lithium atom migrates from an initial site to a neighboring vacant lithium site along these two migration paths as shown in Fig. 4(a) and (b). The migrating lithium atom and distanced atoms are fixed, and all the other atoms and cell sizes are fully relaxed. To check the cell size effect in the calculation, we consider different cell sizes, 108 ($3 \times 3 \times 1$ super cell) and 2400 atoms ($10 \times 10 \times 2$ super cell). The size effect is negligible, as shown in Fig. 4.

The present potential predicts the migration energy barrier to be around 0.8 eV for the ODH and 0.4 eV for the TSH. DFT (LDA) calculation of Van der Ven and Ceder [58] is 0.8 eV (ODH) and 0.23–0.6 eV (TSH). More recently, Ning et al. [60] point out that the LDA calculation overestimates the lithium migration energy barrier in layered $LiCoO_2$ and report the value 0.39 eV (ODH) through a GGA + U calculation. Zhu et al. [61] and Andriyevsky et al. [62] report similar values using the GGA + U, 0.3 and 0.44 eV, respectively. Li et al. [56] calculate the lithium migration energy barrier according to the TSH mechanism using the GGA + U method and obtained the value 0.21 eV. Kang et al. [63] report through a GGA DFT study that the barrier for Li migration in layered $Li(Ni_{0.5}Mn_{0.5})O_2$ is sensitively depends on the interlayer distance, that is, the barrier increases as the interlayer distance decreases. The present potential underestimates the lattice parameter c of layered $LiCoO_2$ as shown in Table 5. Thus, the overestimated migration energy barrier from our potential is consistent with the DFT report of Kang et al. [63]. Our result and the previously reported values based on DFT calculations indicate that the existence of the vacancy sites around the hopping Li ion reduces the migration energy barrier in layered $LiCoO_2$ significantly. Experimentally, the migration energy barrier is reported as being 0.3 [64] and 0.32 eV [65].

The properties discussed above (lattice parameters, elastic constants, enthalpy of formation and lithium migration energy barrier)

are the properties used for parameter fitting. Our results confirm that the Li-Co-O ternary potential parameters are sufficiently well optimized. The other group of properties, not used for fitting but examined to check the transferability of the developed potential, are the redox potential and defect formation energy. The redox potential describes the voltage needed to extract Li atoms out of a bulk system, and is calculated using the expression given in Refs. [66,67]. Table 7 summarizes the calculated redox potential in comparison with experimental data [68–70] and DFT calculations [66,67]. For layered and spinel $LiCoO_2$, the calculated redox potential associated with half delithiation ($LiCoO_2/Li_{0.5}CoO_2$), 3.347 (layered) and 3.069 V (spinel), somewhat underestimates the experimental value, 3.9–4.2 (layered) and 3.3–3.9 V (spinel) [68–70]. The DFT calculations show a discrepancy depending on the approximation method (LDA [66], GGA, GGA + *U* and HSE06 [67]), as shown in Table 7. The underestimation of the redox potential had also been observed for lithium manganese oxides in our recent work on the Li-Mn-O system [20] using the same potential model. We infer that the underestimated redox potential comes from the formalism of our potential model intrinsically, not from the choice of parameter set. DFT calculations using the GGA method also generally underestimate the redox potential of transition metal oxides, and can reproduce correct values only when adopting an optimal *U* value of transition metal ion, which calibrates the electrostatic interaction of *d*-orbital electrons. The present potential model only considers 1*s*-orbital electrostatic interactions for mathematical simplification, and may need to be modified in a way to consider the electrostatic interaction of 3*d*-orbitals to be able to compute the redox potential more accurately.

Finally, we check whether the developed potential reproduces the defect properties well. We calculate the defect formation energies of the layered $LiCoO_2$ for point defects (Frenkel defects and cation anti-site defect) and planar defects (low-index surfaces), and compare them with DFT calculations [53,71–77] and another empirical model (Born + Shell model) [4]. Table 8 summarizes the calculation results. The X Frenkel defect is a pair of an X vacancy and an X interstitial defect (at tetrahedral site) and the cation anti-site ($Co_{Li}Li_{Co}$) defect is a pair of a Li atom in a Co site and a Co atom in a Li site. We calculate the point defect formation energies according to the relative distance (*isolated* or *neighboring*) between two component defects. The literature data for point defects correspond to the *isolated* case. Our calculation for the point defect formation energies is generally in good agreement with other calculations. For the planar defect, we consider (0 0 0 1), (0 1 $\bar{1}$ 0) and (1 1 $\bar{2}$ 0) surfaces. The (0 0 0 1) surface is a polar type, which has different termination on both sides. We rearrange some of the lithium atoms on one side to the opposite side to make both sides the same, as in Refs. [53,75,77]. The (0 1 $\bar{1}$ 0) and (1 1 $\bar{2}$ 0) surfaces are a non-polar type, which has all equivalent layers, so the termination is uniquely defined. The calculated (0 0 0 1) surface energy well matches with the reference data, while the calculated (0 1 $\bar{1}$ 0) and (1 1 $\bar{2}$ 0) surface energy somewhat underestimates the reference data. Our potential reproduces the relative stability between the surfaces well. It needs to be also mentioned here that the (0 0 0 1) surface involves broken bonds of Li, while (0 1 $\bar{1}$ 0) and (1 1 $\bar{2}$ 0) surfaces involve both Li and Co broken bonds. The relative worse estimation of the (0 1 $\bar{1}$ 0) and (1 1 $\bar{2}$ 0) surface energy indicates that the present potential for the Co-O system may have a room for further improvement in future works.

3.4. Reliability of the potential for finite temperature simulation

The properties listed above are calculated at 0 K for the evaluation of the developed potential. In practical applications, however, the potential is mainly utilized for MD simulations at finite temperatures. Some incomplete potentials often fail to perform the finite temperature simulation accompanied by a transformation of the structure into an unknown structure. In this case, if the energy decreases to an extent that the unknown structure becomes a thermodynamically stable phase, the potential is not reliable, at least in that compositional range. It is necessary to test whether the developed potential performs well at finite temperatures, meaning that any undesirable phase transformation does not occur. Therefore, we perform a test simulation that heats and cools the samples to analyze the change in energy and structure for all compound phases. The MD simulation is conducted using our in-house code, as mentioned already. In this code, temperature and pressure are controlled by the Velocity Rescaling method and the Parrinello-Rahman *NpT* ensemble, respectively. The time step used in this simulation is 0.0002 ps, and periodic boundary conditions are applied into all directions. The samples contain about 2000–4000 atoms, temperature is increased by 200 K from 0 to 3000 K. The simulation time is 10 ps per each temperature. Then, the heated sample at each temperature is rapidly cooled to 0 K to check whether the structure is maintained or transformed. If the energy of the rapidly cooled sample recovers the initial energy, one may think that the undesirable phase transformation does not occur during the simulation.

Fig. 5 shows the change in internal energy of cobalt oxide phases and lithium cobalt oxide phases obtained from the above-described simulation as a function of temperature. The solid symbols in Fig. 5 represent the energy during heating, and the open symbols represent the energy after rapid cooling to 0 K from each temperature. Most cobalt oxide phases exhibit a monotonic increase in energy as the temperature increases and recover the initial 0 K energy after rapid cooling, which is a desirable result. Although some transformations involving a decrease in energy occur for the metastable CoO B4 and hypothetical Co_5O_8, these are not considered problematic because the decrease in energy does not exceed the criterion that a wrong phase should not be the most stable phase at the corresponding composition. As in the Co-O system, we confirm that the developed ternary Li-Co-O potential is reliable at finite temperatures. The energy of all compounds monotonically increases during heating and recovers the initial energy after rapid cooling to 0 K. The small increase of energy in rapidly cooled ternary oxide samples is due to local defects introduced during high temperature equilibration and remained during the rapid cooling and relaxation at 0 K. The further increase of energy at higher temperatures is due to the loss

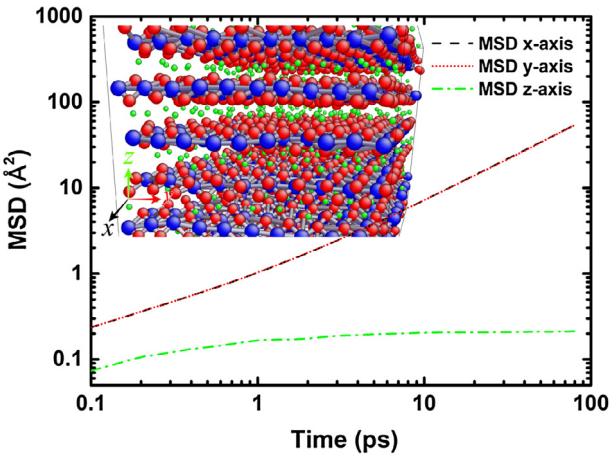

Fig. 6. MSD (log-scale) of lithium atoms in $Li_{0.8}CoO_2$ along *x*, *y* and *z*-axes at 1000 K as a function of time (log-scale) and snapshot of layered $Li_{0.8}CoO_2$ structure during MD simulation at 1000 K.

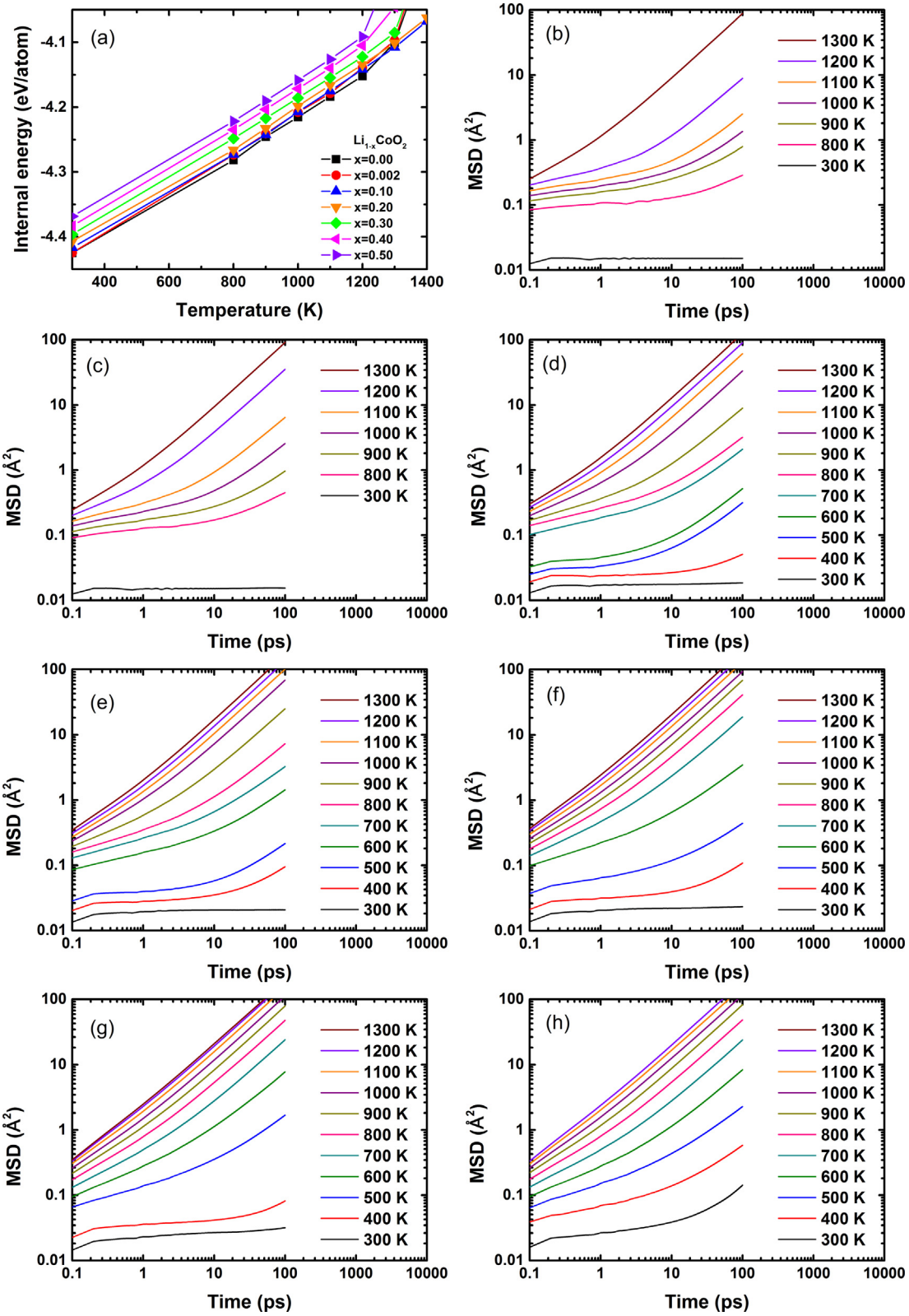

Fig. 7. (a) Energy of layered $Li_{1-x}CoO_2$ as a function of temperature and MSD (log-scale) of lithium atoms in $Li_{1-x}CoO_2$ at each temperature where (b) $x = 0$, (c) $x = 0.002$, (d) $x = 0.1$, (e) $x = 0.2$, (f) $x = 0.3$, (g) $x = 0.4$ and (h) $x = 0.5$ as a function of time (log-scale).

of crystallinity (melting). From the result of this simulation, we confirm that our Co-O binary and Li-Co-O ternary potential is reliable for dynamics simulations in a wide temperature range without causing any undesirable phase transformations (an appearance of an unknown structure as a stable phase).

4. Diffusion of lithium in layered $Li_{1-x}CoO_2$

The diffusion of lithium in the cathode is determinant on the charge/discharge rate of the LIB. During the charge/discharge process, the stoichiometry of cathode materials varies by the delithia-

tion/lithiation reaction, but the effect of the stoichiometry on the diffusion properties is not well-known experimentally and theoretically. Thus, to investigate lithium diffusion properties in layered $Li_{1-x}CoO_2$ according to the lithium composition, we perform diffusion simulations using the developed potential. We use samples of layered $Li_{1-x}CoO_2$ (x = 0, 0.002, 0.1, 0.2, 0.3, 0.4 and 0.5) containing about 2400 atoms, carry out the simulations at temperatures from 300 to 1400 K for 1000 ps.

The mean-squared displacement (MSD) of lithium atoms is calculated from trajectories of samples gathered at every 0.1 ps. We calculate the average of the MSD values for 10 sections divided from the data for 1000 ps to reduce statistical error. It should be noted that most experimental investigations indicate that lithium atoms in a layered $Li_{1-x}CoO_2$ structure diffuse only along the x- and y-axes, i.e. a plane parallel to the Li- and CoO_2-layers. Fig. 6 shows a snapshot of a layered $Li_{0.8}CoO_2$ structure during MD simulation at 1000 K as a representative example, together with the MSD of lithium atoms in $Li_{0.8}CoO_2$ along the x-, y- and z-axes at 1000 K. The MSD curves for the x- and y-axes linearly increase with time, while that for the z-axis becomes flat, which means lithium atoms diffuse only in the same layer (xy plane) and do not cross the CoO_2 layer (along the z-axis). Fig. 7(a) shows the change in internal energy of the $Li_{1-x}CoO_2$ samples, indicating that the structures of the $Li_{1-x}CoO_2$ phases are maintained up to 1200–1400 K. Fig. 7(b)–(h) present the calculated MSDs of lithium atoms in $Li_{1-x}CoO_2$ samples at each temperature. The MSD curve at temperatures below 500–800 K is flat, meaning noticeable diffusion is difficult to observe at low temperatures within a general MD time scale. From the increase in the MSD curve at higher temperatures, it can be confirmed that lithium atoms diffuse inside the layered structure. As can be simply predicted, the diffusion of lithium atoms occurs actively as the lithium vacancy concentration increases.

The diffusion coefficient of lithium (D_{Li}) is calculated for quantitative comparison with experimental information. D_{Li} is obtained from the MSD data using Einstein's relation. In the layered structure, a lithium atom can migrate through two-dimensional channels (within the same layer), so we consider MSD data for only the x- and y-axes. Fig. 8 shows the calculated D_{Li} (log-scale) in $Li_{1-x}CoO_2$ as a function of temperature (reciprocal-scale). The D_{Li} for x = 0 and 0.002 at temperatures below 800 K cannot be calculated since the MSD is almost constant. For the same reason, D_{Li} at 300 K for all compositions cannot be directly obtained from MSD data. However, since the experimental values [78] are those measured at room temperature, we extrapolate our data to estimate the D_{Li} at 300 K. The estimated values for D_{Li} of layered $Li_{1-x}CoO_2$ at 300 K are within the range of 10^{-12}–10^{-14} m^2/s, as shown in Fig. 8, where x varies from 0.5 to 0.1. The present calculation is in good agreement with the experimental values [78], $7 \pm 2 \times 10^{-14}$ m^2/s, obtained by muon-spin spectroscopy for $Li_{0.73}CoO_2$ samples. The estimation for D_{Li} of $Li_{1-x}CoO_2$ (x = 0 and 0.002) at room temperature is in the order of 10^{-20} m^2/s, but it may somewhat disagree with the actual value since it is extrapolated from data points relatively far apart from room temperature. It is interpreted that lithium diffusion is significantly reduced, since the diffusion occurs through the ODH mechanism with a higher energy barrier when the vacancy sites are insufficient around the hopping lithium atom.

From the temperature dependency of the calculated D_{Li}, the activation energy (E_a) of lithium migration can be obtained through the Arrhenius equation, that is, the slope of $\log D_{Li}$ vs $1/T$ plot in Fig. 8. Fig. 9 shows the calculated activation energy as a function of the lithium vacancy concentration. It is clearly shown that the activation energy is significantly different according to the lithium vacancy concentration. The calculated activation energy of $Li_{1-x}CoO_2$ ($0.1 < x < 0.5$) is around 0.3–0.4 eV, which is in good agreement with the experimental value of 0.3 [64] and 0.32 eV [65]. In the case of x = 0 and 0.002, the value is about 0.7–0.8 eV, which is supposed to correspond to the migration energy barrier for ODH. Generally, the E_a calculated from MD simulation at finite temperatures has a lower value than the migration energy barrier calculated by directly moving a lithium atom at 0 K, because the MD simulation at finite temperature contains thermal fluctuations and vacancy sites. The activation energy obtained from the finite temperature MD simulations, 0.3–0.4 eV ($0.1 < x < 0.5$) and 0.7–0.8 eV (x = 0 and 0.002), is slightly lower than the migration energy barrier at 0 K, 0.4 eV for TSH and 0.8 eV for ODH, respectively. The results indicate that the governing mechanism of lithium migration changes depending on the vacancy concentration: from the ODH at low vacancy concentrations ($x < 0.1$) to the TSH at high vacancy concentrations ($x > 0.1$).

It has been shown that the developed interatomic potential of the Li-Co-O system describes the Li diffusion behavior in the $Li_{1-x}CoO_2$ reasonably well. It should be mentioned here that the interatomic potential of the Li-Mn-O system had also been developed through a similar approach and that of the Li-Ni-O system is ongoing. Combining the ternary potentials would enable large-scale atomistic simulations to predict the diffusion, phase transition and defect properties of the Li-(Co, Mn, Ni)-O multi-component system and would provide useful insight into atomic-scale dynamic behavior in developments of new LIB cathode materials. The diffusion simulation code used in this study also is imple-

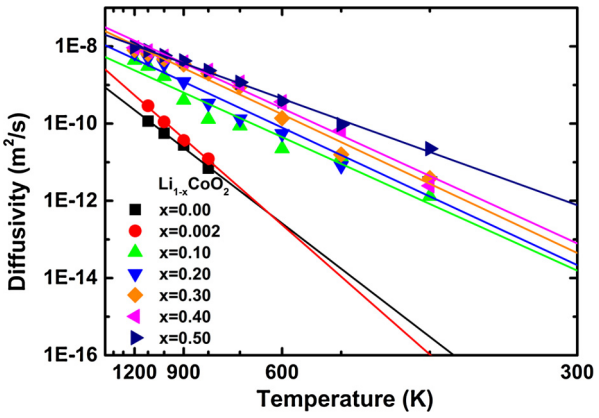

Fig. 8. Diffusion coefficient of lithium in layered $Li_{1-x}CoO_2$ as a function of temperature.

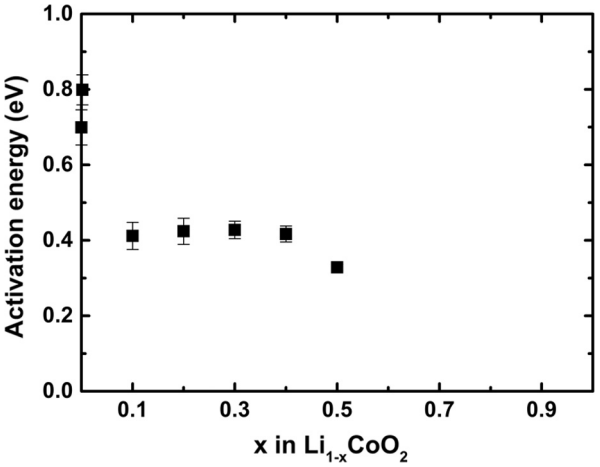

Fig. 9. Activation energy for lithium diffusion in layered $Li_{1-x}CoO_2$ phases.

mented in the iBat simulation platform (http://battery.vfab.org), which provides various multi-scale simulation techniques for LIB materials.

5. Conclusion

The potential developed for the Li-Co-O system reproduces the various fundamental material properties of cobalt oxide and lithium cobalt oxide compounds in reasonable agreements with experimental data and DFT calculations. The calculated diffusion properties are self-consistent and are in good agreement with experimental information. The calculation shows that the lithium diffusion coefficient and the activation energy for lithium migration in layered $Li_{1-x}CoO_2$ are significantly influenced by lithium vacancy concentration. The governing mechanism of diffusion in $Li_{1-x}CoO_2$ is dependent on the lithium vacancy concentration, varying from the ODH at low concentrations to the TSH at high concentrations.

Acknowledgements

This research was supported by the Industrial Strategic Technology Development Program (Grant No. 10041589), funded by the Ministry of Trade, Industry and Energy of Korea.

Appendix A. Supplementary material

Supplementary data associated with this article can be found, in the online version, at https://doi.org/10.1016/j.commatsci.2017.10.010.

References

[1] C.-H. Doh, D.-H. Kim, H.-S. Kim, H.-M. Shin, Y.-D. Jeong, S.-I. Moon, B.-S. Jin, S.-W. Eom, H.-S. Kim, K.-W. Kim, D.-H. Oh, A. Veluchamy, Thermal and electrochemical behaviour of C/Li_xCoO_2 cell during safety test, J. Power Sour. 175 (2008) 881–885, https://doi.org/10.1016/j.jpowsour.2007.09.102.
[2] D. Belov, M.-H. Yang, Investigation of the kinetic mechanism in overcharge process for Li-ion battery, Solid State Ion. 179 (2008) 1816–1821, https://doi.org/10.1016/j.ssi.2008.04.031.
[3] S. Takai, K. Yoshioka, H. Iikura, M. Matsubayashi, T. Yao, T. Esaka, Tracer diffusion coefficients of lithium ion in $LiMn_2O_4$ measured by neutron radiography, Solid State Ion. 256 (2014) 93–96, https://doi.org/10.1016/j.ssi.2014.01.013.
[4] C.A.J. Fisher, M.S. Islam, H. Moriwake, Atomic level investigations of lithium ion battery cathode materials, J. Phys. Soc. Japan 79 (2010) 59–64, https://doi.org/10.1143/JPSJS.79SA.59.
[5] S. Kerisit, A.M. Chaka, T.C. Droubay, E.S. Ilton, Shell model for atomistic simulation of lithium diffusion in mixed Mn/Ti oxides, J. Phys. Chem. C. 118 (2014) 24231–24239, https://doi.org/10.1021/jp506025k.
[6] C. Tealdi, C. Spreafico, P. Mustarelli, Lithium diffusion in $Li_{1-x}FePO_4$: the effect of cationic disorder, J. Mater. Chem. 22 (2012) 24870–24876, https://doi.org/10.1039/c2jm35585j.
[7] S. Lee, S.S. Park, Structure, defect chemistry, and lithium transport pathway of lithium transition metal pyrophosphates ($Li_2MP_2O_7$, M: Mn, Fe, and Co): atomistic simulation study, Chem. Mater. 24 (2012) 3550–3557, https://doi.org/10.1021/cm301921d.
[8] S. Lee, S.S. Park, Atomistic simulation study of mixed-metal oxide ($LiNi_{1/3}Co_{1/3}Mn_{1/3}O_2$) cathode material for lithium ion battery, J. Phys. Chem. C 116 (2012) 6484–6489.
[9] T.X.T. Sayle, F. Caddeo, N.O. Monama, K.M. Kgatwane, P.E. Ngoepe, D.C. Sayle, Origin of electrochemical activity in nano-Li_2MnO_3; stabilization via a "Point Defect Scaffold", Nanoscale 7 (2015) 1167–1180, https://doi.org/10.1039/C4NR05551A.
[10] K. Tateishi, D. Du Boulay, N. Ishizawa, The effect of mixed mn valences on Li migration in $LiMn_2O_4$ spinel. A molecular dynamics study, Appl. Phys. Lett. 84 (2004) 529–531, https://doi.org/10.1063/1.1644320.
[11] S. Lee, J. Park, A.M. Sastry, W. Lu, Molecular dynamics simulations of SOC-dependent elasticity of $Li_xMn_2O_4$ spinels in Li-Ion batteries, J. Electrochem. Soc. 160 (2013) A968–A972, https://doi.org/10.1149/2.147306jes.
[12] R. Fallahzadeh, N. Farhadian, Molecular dynamics simulation of lithium ion diffusion in $LiCoO_2$ cathode material, Solid State Ion. 280 (2015) 10–17, https://doi.org/10.1016/j.ssi.2015.07.001.
[13] A.C.T. van Duin, S. Dasgupta, F. Lorant, W.A. Goddard III, ReaxFF: a reactive force field for hydrocarbons, J. Phys. Chem. A 105 (2001) 9396–9409.
[14] T.P. Senftle, S. Hong, M.M. Islam, S.B. Kylasa, Y. Zheng, Y.K. Shin, C. Junkermeier, R. Engel-Herbert, M.J. Janik, H.M. Aktulga, T. Verstraelen, A. Grama, A.C.T. van Duin, The ReaxFF reactive force-field: development, applications and future directions, NPJ Comput. Mater. 2 (15011) (2016) 1–14, https://doi.org/10.1038/npjcompumats.2015.11.
[15] T. Liang, T.-R. Shan, Y.-T. Cheng, B.D. Devine, M. Noordhoek, Y. Li, Z. Lu, S.R. Phillpot, S.B. Sinnott, Classical atomistic simulations of surfaces and heterogeneous interfaces with the charge-optimized many body (COMB) potentials, Mater. Sci. Eng. R 74 (2013) 255–279, https://doi.org/10.1016/j.mser.2013.07.001.
[16] T. Liang, Y.K. Shin, Y.-T. Cheng, D.E. Yilmaz, K.G. Vishnu, O. Verners, C. Zou, S.R. Phillpot, S.B. Sinnott, A.C.T. van Duin, Reactive potentials for advanced atomistic simulations, Annu. Rev. Mater. Res. 43 (2013) 109–129, https://doi.org/10.1146/annurev-matsci-071312-121610.
[17] F. Kong, H. Zhang, R.C. Longo, B. Lee, D.H. Yeon, J. Yoon, J.H. Park, S.G. Doo, K. Cho, A large-scale simulation method on complex ternary Li-Mn-O compounds for Li-ion battery cathode materials, Comput. Mater. Sci. 112 (2016) 193–204, https://doi.org/10.1016/j.commatsci.2015.10.027.
[18] F. Kong, R.C. Longo, C. Liang, D.H. Yeon, Y. Zheng, J.H. Park, S.G. Doo, K. Cho, CT-MEAM interatomic potential of the Li-Ni-O ternary system for Li-ion battery cathode materials, Comput. Mater. Sci. 127 (2017) 128–135, https://doi.org/10.1016/j.commatsci.2016.10.030.
[19] E. Lee, K.-R. Lee, M.I. Baskes, B.-J. Lee, A modified embedded-atom method interatomic potential for ionic systems: 2NNMEAM+Qeq, Phys. Rev. B 93 (144110) (2016) 1–21, https://doi.org/10.1103/PhysRevB.93.144110.
[20] E. Lee, K.-R. Lee, B.-J. Lee, Interatomic potential of Li-Mn-O and molecular dynamics simulations on Li diffusion in spinel $Li_{1-x}Mn_2O_4$, J. Phys. Chem. C 121 (2017) 13008–13017, https://doi.org/10.1021/acs.jpcc.7b02727.
[21] B.-J. Lee, M.I. Baskes, Second nearest-neighbor modified embedded-atom-method potential, Phys. Rev. B 62 (2000) 8564–8567.
[22] B.-J. Lee, W.-S. Ko, H.-K. Kim, E.-H. Kim, The modified embedded-atom method interatomic potentials and recent progress in atomistic simulations, Calphad 34 (2010) 510–522, https://doi.org/10.1016/j.calphad.2010.10.007.
[23] M.I. Baskes, Modified embedded-atom potentials for cubic materials and impurities, Phys. Rev. B 46 (1992) 2727–2742.
[24] M.I. Baskes, R.A. Johnson, Modified embedded atom potentials for HCP metals, Model. Simul. Mater. Sci. Eng. 2 (1994) 147–163.
[25] M.I. Baskes, Determination of modified embedded atom method parameters for nickel, Mater. Chem. Phys. 50 (1997) 152–158, https://doi.org/10.1016/S0254-0584(97)80252-0.
[26] Y.-M. Kim, I.-H. Jung, B.-J. Lee, Atomistic modeling of pure Li and Mg–Li system, Model. Simul. Mater. Sci. Eng. 20 (035005) (2012) 1–13, https://doi.org/10.1088/0965-0393/20/3/035005.
[27] W.-P. Dong, H.-K. Kim, W.-S. Ko, B.-M. Lee, B.-J. Lee, Atomistic modeling of pure Co and Co-Al system, Calphad 38 (2012) 7–16, https://doi.org/10.1016/j.calphad.2012.04.001.
[28] Y.-M. Kim, Y.-H. Shin, B.-J. Lee, Modified embedded-atom method interatomic potentials for pure Mn and the Fe–Mn system, Acta Mater. 57 (2009) 474–482, https://doi.org/10.1016/j.actamat.2008.09.031.
[29] B.-J. Lee, J.-H. Shim, M.I. Baskes, Semiempirical atomic potentials for the fcc metals Cu, Ag, Au, Ni, Pd, Pt, Al, and Pb based on first and second nearest-neighbor modified embedded atom method, Phys. Rev. B 68 (144112) (2003) 1–11, https://doi.org/10.1103/PhysRevB.68.144112.
[30] A.K. Rappe, W.A. Goddard III, Charge equilibration for molecular dynamics simulations, J. Phys. Chem. 95 (1991) 3358–3363.
[31] F.H. Streitz, J.W. Mintmire, Electrostatic potential for metal-oxide surfaces and interfaces, Phys. Rev. B 50 (1994) 11996–12003.
[32] R.A. Nistor, J.G. Polihronov, M.H. Müser, N.J. Mosey, A generalization of the charge equilibration method for nonmetallic materials, J. Chem. Phys. 125 (094108) (2006) 1–10, https://doi.org/10.1063/1.2346671.
[33] G. Kresse, J. Furthmüller, Efficiency of ab-initio total energy calculations for metals and semiconductors using a plane-wave basis set, Comput. Mater. Sci. 6 (1996) 15–50, https://doi.org/10.1016/0927-0256(96)00008-0.
[34] G. Kresse, D. Joubert, From ultrasoft pseudopotentials to the projector augmented-wave method, Phys. Rev. B 59 (1999) 1758–1775, https://doi.org/10.1103/PhysRevB.59.1758.
[35] J.P. Perdew, K. Burke, M. Ernzerhof, Generalized gradient approximation made simple, Phys. Rev. Lett. 77 (1996) 3865–3868, https://doi.org/10.1103/PhysRevLett. 77.3865.
[36] P.E. Blöchl, O. Jepsen, O.K. Andersen, Improved tetrahedron method for Brillouin-zone integrations, Phys. Rev. B 49 (1994) 16223–16233, https://doi.org/10.1103/PhysRevB.49.16223.
[37] A. Jain, S.P. Ong, G. Hautier, W. Chen, W.D. Richards, S. Dacek, S. Cholia, D. Gunter, D. Skinner, G. Ceder, K.A. Persson, Commentary: the materials project: a materials genome approach to accelerating materials innovation, APL Mater. 1 (011002) (2013) 1–11, https://doi.org/10.1063/1.4812323.
[38] A.K. Niessen, A.R. Miedema, F.R. de Boer, R. Boom, Enthalpies of formation of liquid and solid binary alloys based on 3d metals IV. Alloys of cobalt, Physica B 151 (1988) 401–432, https://doi.org/10.1016/0378-4363(88)90296-3.
[39] M. Chen, B. Hallstedt, L.J. Gauckler, Thermodynamic assessment of the Co-O system, J. Phase Equilib. 24 (2003) 212–227, https://doi.org/10.1111/j.1551-2916.2004.00683.x.

[40] R.W. Grimes, K.P.D. Lagerlöf, Polymorphs of cobalt oxide, J. Am. Ceram. Soc. 74 (1991) 270–273, https://doi.org/10.1111/j.1151-2916.1991.tb06873.x.
[41] M.J. Redman, E.G. Steward, Cobaltous oxide with the zinc blende/wurtzite-type crystal structure, Nature 193 (1962), https://doi.org/10.1038/193867a0, 867–867.
[42] V.A.M. Brabers, A.D.D. Broemme, Low-spin-high-spin transition in the Co_3O_4 spinel, J. Magn. Magn. Mater. 104–107 (1992) 405–406, https://doi.org/10.1016/0304-8853(92)90853-G.
[43] P.E. Tomaszewski, Structural phase transitions in crystals. I. Database, Phase Trans. 38 (1992) 127–220, https://doi.org/10.1080/01411599208222899.
[44] J. Chenavas, J.C. Joubert, M. Marezio, Low-spin → high-spin state transition in high pressure cobalt sesquioxide, Solid State Commun. 9 (1971) 1057–1060, https://doi.org/10.1016/0038-1098(71)90462-5.
[45] H.R. Oswald, M.J. Wampetich, Die Kristallstrukturen von Mn_5O_8 und $Cd_2Mn_3O_8$, Helv. Chim. Acta 50 (1967) 2023–2034, https://doi.org/10.1002/hlca.19670500736.
[46] X. Wang, I. Loa, K. Kunc, K. Syassen, M. Amboage, Effect of pressure on the structural properties and Raman modes of $LiCoO_2$, Phys. Rev. B 72 (224102) (2005) 1–8, https://doi.org/10.1103/PhysRevB.72.224102.
[47] M. Wang, A. Navrotsky, Enthalpy of formation of $LiNiO_2$, $LiCoO_2$ and their solid solution, $LiNi_{1-x}Co_xO_2$, Solid State Ion. 166 (2004) 167–173, https://doi.org/10.1016/j.ssi.2003.11.004.
[48] R.J. Gummow, D.C. Liles, M.M. Thackeray, Spinel versus layered structures for lithium cobalt oxide synthesised at 400 °C, Mater. Res. Bull. 28 (1993) 235–246, https://doi.org/10.1016/0025-5408(93)90157-9.
[49] M. Catti, G. Sandrone, Ab initio study of corundum-like Me_2O_3 oxides (Me = Ti, V, Cr, Fe Co, Ni), Faraday Discuss. 106 (1997) 189–203.
[50] N. Uchida, S. Saito, Elastic constants and acoustic absorption coefficients in MnO, CoO, and NiO single crystals at room temperature, J. Acoust. Soc. Am. 51 (1972) 1602–1605, https://doi.org/10.1121/1.1913005.
[51] J.N. Reimers, J.R. Dahn, Electrochemical and in situ X-ray diffraction studies of lithium intercalation in Li_xCoO_2, J. Electrochem. Soc. 139 (1996) 2091–2097.
[52] Y. Takahashi, N. Kijima, K. Tokiwa, T. Watanabe, J. Akimoto, Single-crystal synthesis, structure refinement and electrical properties of $Li_{0.5}CoO_2$, J. Phys. Condens. Matter. 19 (436202) (2007) 1–12, https://doi.org/10.1088/0953-8984/19/43/436202.
[53] D. Kramer, G. Ceder, Tailoring the morphology of $LiCoO_2$: a first principles study, Chem. Mater. 21 (2009) 3799–3809, https://doi.org/10.1021/cm9008943.
[54] M. Catti, Ab initio study of Li^+ diffusion paths in the monoclinic $Li_{0.5}CoO_2$ intercalate, Phys. Rev. B 61 (2000) 1795–1803, https://doi.org/10.1103/PhysRevB.61.1795.
[55] M. Wang, A. Navrotsky, S. Venkatraman, A. Manthiram, Enthalpy of formation of $LixCoO_2$ ($0.5 \leq x \leq 1.0$), J. Electrochem. Soc. 152 (2005) J82–J84, https://doi.org/10.1149/1.1931292.
[56] G. Li, S. Zhou, P. Wang, J. Zhao, Halogen-doping in $LiCoO_2$ cathode materials for Li-ion Batteries. Insights from ab initio calculations, R. Soc. Chem. Adv. 5 (2015) 107326–107332, https://doi.org/10.1039/C5RA21258H.
[57] A. Van der Ven, M. Aydinol, G. Ceder, G. Kresse, J. Hafner, First-principles investigation of phase stability in Li_xCoO_2, Phys. Rev. B 58 (1998) 2975–2987, https://doi.org/10.1103/PhysRevB.58.2975.
[58] A. Van Der Ven, G. Ceder, Lithium diffusion in layered Li_xCoO_2, Electrochem. Solid-State Lett. 3 (2000) 301–304, https://doi.org/10.1149/1.1391130.
[59] A. Van der Ven, G. Ceder, Lithium diffusion mechanisms in layered intercalation compounds, J. Power Sour. 97–98 (2001) 529–531, https://doi.org/10.1016/S0378-7753(01)00638-3.
[60] F. Ning, S. Li, B. Xu, C. Ouyang, Strain tuned Li diffusion in $LiCoO_2$ material for Li ion batteries. A first principles study, Solid State Ion. 263 (2014) 46–48, https://doi.org/10.1016/j.ssi.2014.05.008.
[61] X. Zhu, C.S. Ong, X. Xu, B. Hu, J. Shang, H. Yang, S. Katlakunta, Y. Liu, X. Chen, L. Pan, J. Ding, R.W. Li, Direct observation of lithium-ion transport under an electrical field in Li_xCoO_2 nanograins, Sci. Rep. 3 (2013), 1084 1 8 10.1038/srep01084.
[62] B. Andriyevsky, K. Doll, T. Jacob, Electronic and transport properties of $LiCoO_2$, Phys. Chem. Chem. Phys. 16 (2014) 23412–23420, https://doi.org/10.1039/C4CP03052D.
[63] K. Kang, Y.S. Meng, J. Bréger, C.P. Grey, G. Ceder, Electrodes with high power and high capacity for rechargeable lithium batteries, Science 311 (2006) 977–980, https://doi.org/10.1126/science.1122152.
[64] K. Nakamura, H. Ohno, K. Okamura, Y. Michihiro, T. Moriga, I. Nakabayashi, T. Kanashiro, ^7Li NMR study on Li^+ ionic diffusion and phase transition in Li_xCoO_2, Solid State Ion. 177 (2006) 821–826, https://doi.org/10.1016/j.ssi.2006.02.021.
[65] M. Okubo, Y. Tanaka, H. Zhou, T. Kudo, I. Honma, Determination of activation energy for Li ion diffusion in electrodes, J. Phys. Chem. B 113 (2009) 2840–2847, https://doi.org/10.1021/jp8099576.
[66] M. Aydinol, A. Kohan, G. Ceder, K. Cho, J. Joannopoulos, Ab initio study of lithium intercalation in metal oxides and metal dichalcogenides, Phys. Rev. B 56 (1997) 1354–1365, https://doi.org/10.1103/PhysRevB.56.1354.
[67] D.H. Seo, A. Urban, G. Ceder, Calibrating transition-metal energy levels and oxygen bands in first-principles calculations: accurate prediction of redox potentials and charge transfer in lithium transition-metal oxides, Phys. Rev. B 92 (115118) (2015) 1–11, https://doi.org/10.1103/PhysRevB.92.115118.
[68] R.J. Gummow, M.M. Thackeray, W.I.F. David, S. Hull, Structure and electrochemistry of lithium cobalt oxide synthesised at 400 °C, Mater. Res. Bull. 27 (1992) 327–337, https://doi.org/10.1016/0025-5408(92)90062-5.
[69] E.I. Santiago, A.V.C. Andrade, C.O. Paiva-Santos, L.O.S. Bulhões, Structural and electrochemical properties of $LiCoO_2$ prepared by combustion synthesis, Solid State Ion. 158 (2003) 91–102, https://doi.org/10.1016/S0167-2738(02)00765-8.
[70] G.G. Amatucci, J.M. Tarascon, L.C. Klein, CoO_2, the end member of the Li_xCoO_2 solid solution, J. Electrochem. Soc. 143 (1996) 1114–1123, https://doi.org/10.1149/1.1836594.
[71] Y. Koyama, H. Arai, I. Tanaka, Y. Uchimoto, Z. Ogumi, Defect chemistry in layered $LiMO_2$ (M = Co, Ni, Mn, and $Li_{1/3}Mn_{2/3}$) by first-principles calculations, Chem. Mater. 24 (2012) 3886–3894.
[72] J.A. Santana, J. Kim, P.R.C. Kent, F.A. Reboredo, Successes and failures of Hubbard-corrected density functional theory: the case of Mg doped $LiCoO_2$, J. Chem. Phys. 141 (164706) (2014) 1–11, https://doi.org/10.1063/1.4899040.
[73] K. Hoang, M.D. Johannes, Defect chemistry in layered transition-metal oxides from screened hybrid density functional calculations, J. Mater. Chem. A 2 (2014) 5224–5235, https://doi.org/10.1039/c4ta00673a.
[74] Y. Kim, First-principles investigation of the structural characteristics of $LiMO_2$ cathode materials for lithium secondary batteries, J. Mol. Struct. 1099 (2015) 317–322, https://doi.org/10.1016/j.molstruc.2015.06.058.
[75] L. Hu, Z. Xiong, C. Ouyang, S. Shi, Y. Ji, M. Lei, Z. Wang, H. Li, X. Huang, L. Chen, Ab initio studies on the stability and electronic structure of $LiCoO_2$ (003) surfaces, Phys. Rev. B 71 (125433) (2005) 1–10, https://doi.org/10.1103/PhysRevB.71.125433.
[76] L. Dahéron, H. Martinez, R. Dedryvère, I. Baraille, M. Ménétrier, C. Denage, C. Delmas, D. Gonbeau, Surface properties of $LiCoO_2$ investigated by XPS analyses and theoretical calculations, J. Phys. Chem. C 113 (2009) 5843–5852, https://doi.org/10.1021/jp803266w.
[77] Y. Kim, H. Lee, S. Kang, First-principles and experimental investigation of the morphology of layer-structured $LiNiO_2$ and $LiCoO_2$, J. Mater. Chem. 22 (2012) 12874–12881, https://doi.org/10.1039/c2jm31145c.
[78] J. Sugiyama, K. Mukai, Y. Ikedo, H. Nozaki, M. Månsson, I. Watanabe, Li diffusion in Li_xCoO_2 probed by Muon-Spin spectroscopy, Phys. Rev. Lett. 103 (147601) (2009) 1–5, https://doi.org/10.1103/PhysRevLett. 103.147601.